Mon. Not. R. Astron. Soc. **000**, 000–000 (0000) Printed 3 June 2005 (MN LATEX style file v1.4)

Gas Inflow in Barred Galaxies — Effects of Secondary Bars

Witold Maciejewski[1,2], Peter J. Teuben[3], Linda S. Sparke[4] and James M. Stone[3]
[1] *Theoretical Physics, 1 Keble Road, University of Oxford, Oxford, OX1 3NP,* witold@thphys.ox.ac.uk
[2] *Jagiellonian University Observatory, ul. Orla 171, Kraków, Poland*
[3] *Department of Astronomy, University of Maryland, College Park, MD 20742*
[4] *Department of Astronomy, University of Wisconsin, 475 N Charter St, Madison, WI 53706*

3 June 2005

ABSTRACT
We report here results of high-resolution hydrodynamical simulations of gas flows in barred galaxies, with a focus on gas dynamics in the central kiloparsec. In a single bar with an Inner Lindblad Resonance, we find either near-circular motion of gas in the nuclear ring, or a spiral shock extending towards the galaxy center, depending on the sound speed in the gas. From a simple model of a dynamically-possible doubly barred galaxy with resonant coupling, we infer that the secondary bar is likely to end well inside its corotation. Such a bar cannot create shocks in the gas flow, and therefore will not reveal itself in color maps through straight dust lanes: the gas flows induced by it are different from those caused by the rapidly rotating main bars. In particular, we find that secondary stellar bars are unlikely to increase the mass inflow rate into the galactic nucleus.

Key words: hydrodynamics — shock waves — galaxies: kinematics and dynamics — galaxies: ISM — galaxies: spiral — galaxies: structure — galaxies: nuclei — ISM: kinematics and dynamics

1 INTRODUCTION

Gas in disc galaxies develops sharp and well-defined characteristic morphological features, as a response of this dynamically cold and dissipative medium to the structural details of the underlying gravitational potential. In barred galaxies, the most distinctive of these features is a special category of dust lanes, where the gas and dust get compressed. These often appear as two symmetric, almost straight lanes, slightly tilted to the bar major axis, and located at the leading edge of the bar (Athanassoula 1984). Throughout this paper, we will call them the *principal dust lanes*. Another prominent feature is a set of resonance rings (see e.g. Buta 1986, Buta 1995), which take oval or circular shapes.

Both the theory of orbital structure, and hydrodynamical modeling of gas in barred galaxies, provide a consistent picture that relates the characteristic gas features to the galaxy's dynamics (see Sellwood & Wilkinson 1993 for a review). If the bar has an Inner Lindblad Resonance (ILR), gas can populate the two major families of stable orbits inside the bar: the x_1 orbits elongated with the bar, and x_2 orbits perpendicular to it. Around the radius of the ILR, orbiting gas shifts gradually from the x_1 orbits to the x_2 orbits, creating two *principal shocks* along the leading edges of the bar (Athanassoula 1992). Gas and dust are compressed by the shock, causing large extinction, so we see these regions as the dark *principal dust lanes* in the galaxy image. The shocked gas loses angular momentum to the bar — hydrodynamical models indicate a considerable gas inflow towards the center. If gas follows closely the periodic orbits in the bar (is dynamically cold), it should eventually settle on the nuclear ring (Piner, Stone & Teuben 1995; Patsis & Athanassoula 2000), located approximately at the position of the bar's ILR. By contrast to the principal dust lanes, gas concentrated in the nuclear ring experiences little shear, and star formation is likely to occur there, causing the blue appearance of this ring (Buta 1986).

In this picture, bars provide a mechanism for moving gas from the galactic disk in towards the centre to create a starburst. However, Active Galactic Nuclei (AGN) require mass accretion to extend to within a few parsecs of the galaxy center, much closer in than the usual position of bar's ILR, which usually has a radius at least 10% of that at corotation. If orbits of the gas flow oscillate more freely around the periodic orbits (gas is dynamically warmer), such flow can be driven closer to the galactic center (Englmaier & Gerhard 1997, Patsis & Athanassoula 2000).

Additionally, a mechanism of bars within bars has been invoked to drive further inflow, and thus feed the AGN in a manner similar to the inflow on large scales (Shlosman, Frank & Begelman 1989). It involves a cascade of nested, independently rotating bars, that ensure continuous gas inflow to the very central regions. Arguments for the existence of multiple (or at least double) bars come from both theory

and observations. They emerge as a rather common phenomenon, from a survey of 38 nearby early-type barred field galaxies (Erwin & Sparke 1999), which indicates that at least ∼20% of them possess secondary bars. The inner bar characteristically is 5 to 7 times smaller than the main one. It is oriented randomly with respect to the main bar (Buta & Crocker 1993, Friedli 1996), which one should expect if they are dynamically distinct subsystems. The presence of secondary bars in infrared images, indicates that they are not exclusively made out of gas, but rather contain old stars, and thus form independent systems from the point of view of stellar dynamics. The reason for this may be that orbital times in the inner galaxy are much smaller than those at radii of a few kiloparsecs, and the dynamically decoupled inner bar should rotate faster than the outer structure. Simple analytical models (Maciejewski & Sparke 1997) indicate that periodic feeding of the nucleus may occur in this scenario.

To test this hypothesis, one can follow gas dynamics in combined gas and stars numerical simulations in which such double bars form (*e.g.* Friedli & Martinet 1993, who used Smoothed Particle Hydrodynamics, *i.e.* the SPH algorithm). Nevertheless, the resolution and accuracy achieved so far is rather low. On the other hand, one can assume potentials and pattern speeds of the two stellar bars, and study the gas response (Athanassoula 2000). This paper follows the second approach, but instead of choosing the parameters of the bars arbitrarily, we take them from a dynamically possible model of a doubly barred galaxy (Maciejewski & Sparke 2000, hereafter Paper I), which was constructed by searching for stellar orbits that can support a potential of two nested bars with different rotation periods.

Numerical models of gas flow in barred galaxies can be traced back more than twenty years (see Athanassoula 1992, and Sellwood & Wilkinson 1993 for reviews), but an overwhelming increase in computing speed and memory makes the recent models considerably more detailed, and inclusive of a greater variety of physical phenomena. Despite this progress, the rate of inflow is still not well determined, with methods based on SPH algorithms predicting inflow that is orders of magnitude higher than that in grid-based methods (compare Piner et al. 1995 with Patsis & Athanassoula 2000). A landmark in this field is a set of about two hundred hydrodynamical models, created by Athanassoula (1992) with an Eulerian code. These explore the dependence of the gas flow on various parameters of the model potential. By selecting models that reproduce the observed shape of the principal dust lanes, Athanassoula showed that bar's corotation should be located just past the end of the bar. One can also infer from this set of models that an ILR is necessary for the principal dust lanes to be offset from the center, as seen in many real galaxies.

Piner et al. (1995) repeated some of these calculations with better resolution on a polar grid. They noticed that if an ILR is present, a nuclear ring forms inside this resonance. Virtually no gas passes inside the nuclear ring in their simulation to reach the nucleus. If the ILR is absent the nuclear ring does not form, and strong inflow to the center can take place, as found by Athanassoula (1992), and confirmed by Piner et al. (1995). Englmaier & Gerhard (1997) noticed that the principal shock structure depends on the gas sound speed: the off-axis shock at low sound speed turns into an on-axis one when the sound speed is high. Recently Englmaier & Shlosman (2000) have used a grid-based algorithm in polar coordinates to study gas flows in central parts of barred galaxies.

We use high resolution hydrodynamical simulations to examine in detail the gas flow in barred galaxies, with particular interest in the flows within the inner 1 kpc. In §2, we present our code, and describe the model. In §3, we revise and extend the basic picture of gas flow in a bar, that we outlined above. In §4, we focus our attention on the inner 1 kpc, and explore the nature of the nuclear ring, and gas flow in the presence of a dynamically possible inner secondary bar. We find that although it is not likely that the secondary bar enhances inflow in the inner galaxy, there are other conditions permitting strong inflow. We relate our models to observations in §5.

2 NUMERICAL MODELING OF GAS FLOWS IN GALAXIES

It is difficult to model the interstellar medium (ISM) in galaxies on global scales, because it has a complex morphology that can be traced to sizes many orders of magnitude smaller than the scale of interest (Sellwood & Wilkinson 1993). The gaseous ISM consists of several phases with considerably different physical properties, and is highly turbulent, and probably fractal (see *e.g.* Elmegreen 1997, Padoan, Jones & Nordlund 1997). If a single-fluid approximation is used to model global gas features, this fluid has no commonly accepted equation of state. For this reason a variety of numerical methods has been developed for the study of global ISM dynamics in galaxies — we refer the reader to Teuben (1995) for a review. In this paper, we implement the full solution of the hydrodynamical equations in the Eulerian formulation on a fixed grid.

2.1 Our code, simulation properties, and initial conditions

We used the grid-based Eulerian code CMHOG, written by James M. Stone at the University of Maryland, and briefly described by Piner et al. (1995). It solves the single-fluid hydrodynamic equations in their conservative form, i.e., the continuity equation

$$\frac{\partial \rho}{\partial t} + \nabla \cdot (\rho \mathbf{v}) = 0, \tag{1}$$

and Euler's equation

$$\frac{\partial (\rho \mathbf{v})}{\partial t} + \nabla \cdot (\rho \mathbf{v}\mathbf{v}) = -\nabla P - \rho \nabla \Phi, \tag{2}$$

where the $\mathbf{vv}$ in the second term represents the velocity tensor $T_{ij} = v_i v_j$. The third (energy) hydrodynamic equation is replaced by assuming an isothermal equation of state, which closes the system of equations defining the model. The typical cooling time in the problem is much shorter than the time-step, and the isothermal equation of state forces the gas to cool instantly. The gas temperature is fixed to model the statistical behaviour of gas clouds. Self-gravity of the gas is not taken into account.

The CMHOG code solves the hydrodynamical equations above by implementing the PPM (piecewise parabolic

Table 1. The list of grids

grid name	inner boundary	number of cells tangential	number of cells radial	size of the inner cell
Ls	100 pc	40	67	4.0 pc
Le	20 pc	40	88	0.8 pc
Ms	100 pc	80	132	2.0 pc
Me	20 pc	80	174	0.4 pc
Hs	100 pc	160	261	1.0 pc

method) algorithm (Woodward & Colella 1984) in its Lagrangian remap formulation. The only viscosity in this code is the numerical one, and a test with gas in circular motion has been performed to show that it is too small to noticeably alter the flow within times considered in this work.

The most appropriate grid for disk modeling is a polar one, and Piner et al. (1995) reformulated the CMHOG code to use planar polar coordinates in 2D, which we adopt here. Because the PPM algorithm works best for nearly square grid cells ($\Delta R \simeq R\Delta\varphi$), and since the number of tangential zones is fixed, the cell size is proportional to R. The resolution near the grid center is excellent, so the polar grid is suitable to accurate study of circumnuclear phenomena in galaxies. On the other hand, the time-step, which is related to the cell size by the Courant condition, becomes prohibitively short unless the inner boundary is imposed at a reasonable distance from the grid center. This is a disadvantage of a polar grid, because it requires additional boundary conditions and places the innermost galaxy outside the modeled domain.

Calculations for all our models were performed in two dimensions on polar grids extending outwards to 16 kpc in radius. We do not extend our grids inwards beyond the inner 20 pc (the extended grids Le and Me), and cut them at 100 pc when possible (grids Ls, Ms, and Hs). Grids used in this work are listed in Table 1. In order to achieve the resolution of the Me grid near the center, a Cartesian grid would require $\approx 4\times10^9$ cells, orders of magnitude beyond currently available resources.

We assume that the gas flow is bisymmetric, so we modeled half of the plane only, and we imposed periodic boundary conditions in the azimuthal direction. We considered both free flow and reflective boundaries in the radial direction, but since the circumnuclear gas morphology may depend on the gas entering the grid through the inner boundary, such entering has been prohibited, i.e. on the inner boundary we allow outflow only. The same inner boundary condition is used in all models of Piner et al. (1995), and Englmaier & Shlosman (2000).

The gas in our models is initially distributed uniformly over the grid with a surface density 10 $M_\odot pc^{-2}$, and it orbits at its circular velocity in the initially axisymmetric potential. Here we approximate the gas in a galaxy consisting of a variety of individual clouds as an isothermal single-component fluid. If the temperature of this fluid is interpreted statistically as a measure of the cloud velocity dispersion, as suggested by Englmaier & Gerhard (1997), the cell size has to be larger than the average cloud size to make this approach plausible — it is at least 0.4 pc at the inner boundary of the grid Me. We ran models with the sound speed of 5 or 20 km/s, which corresponds respectively to the velocity dispersion in the Galactic disk inside the solar radius, and the vertical cloud velocity dispersion in the Galactic bulge. Thus a 2 Gyr run corresponds to 0.31 and 1.25 sound-crossing times on our grid respectively, and almost 12 orbits of gas at the corotation radius of the main bar.

2.2 Potential and forces for a double bar

We follow gas flows in the potential of Model 2 constructed in Paper I. This is a model of a dynamically possible doubly barred galaxy. For gas flows in a single bar, the mass of the secondary bar is redistributed into the axisymmetric bulge. The semi-major axis of the main bar is 6 kpc, while that of the secondary bar is 1.2 kpc. The bars rotate rigidly and with uniform speed about the axis perpendicular to the plane of the gas flow. Pattern speeds of the main and secondary bars are 36 km $s^{-1}kpc^{-1}$ and 110 km $s^{-1}kpc^{-1}$ respectively, which corresponds to rotation periods 0.171 Gyr and 0.056 Gyr. The rotation curve of the system with contributions from its components, accompanied by a plot of angular frequencies with pattern speeds of the bars superimposed is presented in Fig.3 of Paper I.

The potential of a single bar is steady in the frame rotating with it, and its forces on the fluid in each grid cell can be calculated at the beginning of the run, and stored for later use. If another, independently rotating bar is present, there is no reference frame in which the potential is steady. Therefore implementation of an additional bar is equivalent to implementing a single bar in any uniformly rotating frame. At the start of the run, for each grid cell we calculate forces F_0 from the part of the potential which is steady in the reference frame rotating with the main bar (*i.e.* from the main bar, disk and bulge). We also calculate the force F_S from the second bar on a grid corotating with this bar, and having the same radial zone spacing, but more nodes in the tangential direction than our computational grid. At any given time, the code finds the relative position of the bars, and interpolates F_S in the tangential direction with the use of splines. The gravitational force from the second bar is added to F_0 to give the total force at any point (R, φ). Runs for a single bar were performed in various reference frames, but runs for a doubly barred galaxy are all in the frame rotating with the primary bar.

In order to avoid spurious shocks and other features that may occur when bars are turned on abruptly, we introduce non-axisymmetric components of the potential gradually by forming them out of the bulge. We keep the sum of the masses of bulge and the bars constant within a given radius (10 kpc here), and also hold the central density constant. The disk parameters do not change while the bars are being introduced. At the start, the bars are absent, and the force is the sum of disk and bulge components. We then introduce the primary bar by allowing it to grow linearly in mass until it reaches its full strength at 0.1 Gyr (at about half of its rotation period), and we analyse the switch-on effects by performing a variation on this run, in which the bar is introduced 5 times more slowly. In models with a secondary bar, we either introduce the inner bar simultaneously with the main one, or we wait till 0.5 Gyr for the gas flow in the main bar to stabilize, and then let the inner bar grow

linearly for another 0.05 Gyr. After both bars have been introduced, the total force F is just the sum of F_0 and F_S.

2.3 Test problems

The CMHOG code passed various standard tests including shock tubes, advection, and the strong shock test suite. The radial outflow, cylindrical shock tubes and uniform rotation were also tested in polar coordinates (see Piner et al. 1995).

We checked how well the code conserves mass and angular momentum, both with an imposed radial gas flow in an axisymmetric potential, and for the flows in our bar models. For the purely radial gas motion, with no rotation, mass is conserved very well. For example, even on lowest resolution grid Ls, in the test case of supersonic radial inflow with a free outflow condition at the inner boundary, the error in mass calculated from fluxes is of the order of 10^{-4} of the total gas mass on the grid, at the time when about 50% of gas on the grid has passed through the boundary. In the models with a single bar on low resolution grid Ls, the mass error is 0.25% of the total mass at the end of the run (2 Gyr). We defined the angular momentum error by the discrepancy between the two sides of equation

$$\frac{d}{dt}\left(\int_{\rm grid} \mathbf{r}\times\mathbf{v}\ \mathbf{dM}\right) = \int_{\rm grid} \mathbf{r}\times\mathbf{F}\ \mathbf{dM}\ -\ \int_{\rm bndry} \mathbf{dl}\ \mathbf{f_L}, \quad (3)$$

with $\mathbf{f_L}$ being the angular momentum flux, $d\mathbf{l}$ a unit vector pointing outward from the grid boundary, $\mathbf{r}\times\mathbf{F}$ the gravitational torque at position $\mathbf{r}$, and $\mathbf{v}$ the gas velocity there. This error varies at the end of the test run from 0.5 to 0.9% of the total value, so it is larger than the mass error, but still small. The mass and angular momentum errors for the runs with double bars are similar to the ones quoted above.

We also compared gas flows in a model with a single bar calculated in a frame rotating with the bar, and in a stationary inertial frame. They show no significant differences, which makes us believe that the time-varying potential was implemented properly in the code.

2.4 General remarks about hydrodynamical models built in this work

About 20 hydrodynamical runs were performed, in potentials of one or two bars for various grids, gas sound speeds, and initial conditions. In this paper, we focus on three setups, with a further one serving as a comparison model; these are listed in Table 2. Run S05 was performed in order to check consistency of our results with those of Athanassoula (1992) and Piner et al. (1995). The gravitational potential in this run differs from Athanassoula's standard model by the Ferrers index of the bar being $n = 2$ here, instead of $n = 1$. The dependence on gas sound speed first reported by Englmaier & Gerhard (1997) was investigated in run S20. The gas flow in a dynamically possible doubly barred galaxy was explored on the basis of run D05 with the low sound speed.

In all the runs, soon after the bars are fully introduced, gas dynamics enters a global steady state, *i.e.* it does not show any major structural changes with time. Features of gas flow in bars presented in the following sections clearly persist throughout the hydrodynamical runs, and therefore are part of this global steady state. Nevertheless, the gas flow is never completely stationary on local scales. All our runs show the formation of density concentrations, that propagate through the shocks, and create blobs and smudges. In the density diagrams, they move fast towards the shock, get shocked, and fall inwards almost along the shock, thickening the density enhancement associated with the shock. The smudge then splits from the shock, forms an arch overshooting the nuclear ring downstream from the shock, and enters the opposite shock. In run S05 this gas density enhancement propagates through the grid with an average period of 88 Myr, about half of the bar rotation period. There is no significant change of its amplitude throughout the run, and many features on the snapshot density diagrams are transient. We performed a number of variations to run S05 on the low resolution grid Ls rotating at various rates, including one in an inertial frame, so that the position of the bar on the grid is no longer fixed. The appearance and periodicity of these features remained unaffected, so we believe that they are not purely numerical effects. We also repeated run S05 on the Ms grid with the bar being introduced more slowly, over 0.5 Gyr or almost 3 rotation periods. This had no significant effect on the overall gas flow morphology, but it did weaken the non-stationary propagating features.

Table 2. The list of physical setups modeled here

setup name	bar	sound speed v_s	grids with ending time
S05	single	5 km s^{-1}	Ls,Ms,Hs 2.0 Gyr
S20	single	20 km s^{-1}	Me 0.9 Gyr
D05	double	5 km s^{-1}	Me 2.0 Gyr
N05	nuclear	5 km s^{-1}	Le 2.0 Gyr

Much more nearly stationary than the density diagrams are the plots where we display the square of velocity divergence in the gas ($div^2\mathbf{v}$) for areas with $div\ \mathbf{v} < 0$. Negative divergence, or convergent flow indicates shocks. Smudges and blobs do not appear in the velocity divergence diagrams, showing that these features do not disturb the velocity field greatly.

3 FUNDAMENTAL FEATURES OF FLOWS IN A SINGLE BAR

General features of gas flow in a single, fast bar with two ILRs can be seen in Fig. 1, which is a snapshot of a run S05 after the flow has entered a steady state. Together with the density distribution, we displayed there the square of velocity divergence in the gas ($div^2\mathbf{v}$) for areas where $div\ \mathbf{v} < 0$, which indicates shocks. The main features of gas flow comply well with the basic paradigm described in the Introduction. Two principal shocks (marked **PS** in Fig.1) on the leading edge of the bar are almost straight, off-centered from the nucleus, and inclined to the bar's major axis. The largest values of $div^2\mathbf{v}$ are detected in these principal shocks, and the velocity field displayed by arrows shows that the gas abruptly changes velocity when crossing the shock. The shocked gas rapidly falls towards the galaxy center: at the radii where shocks are present, gas inflow to the center dominates. In

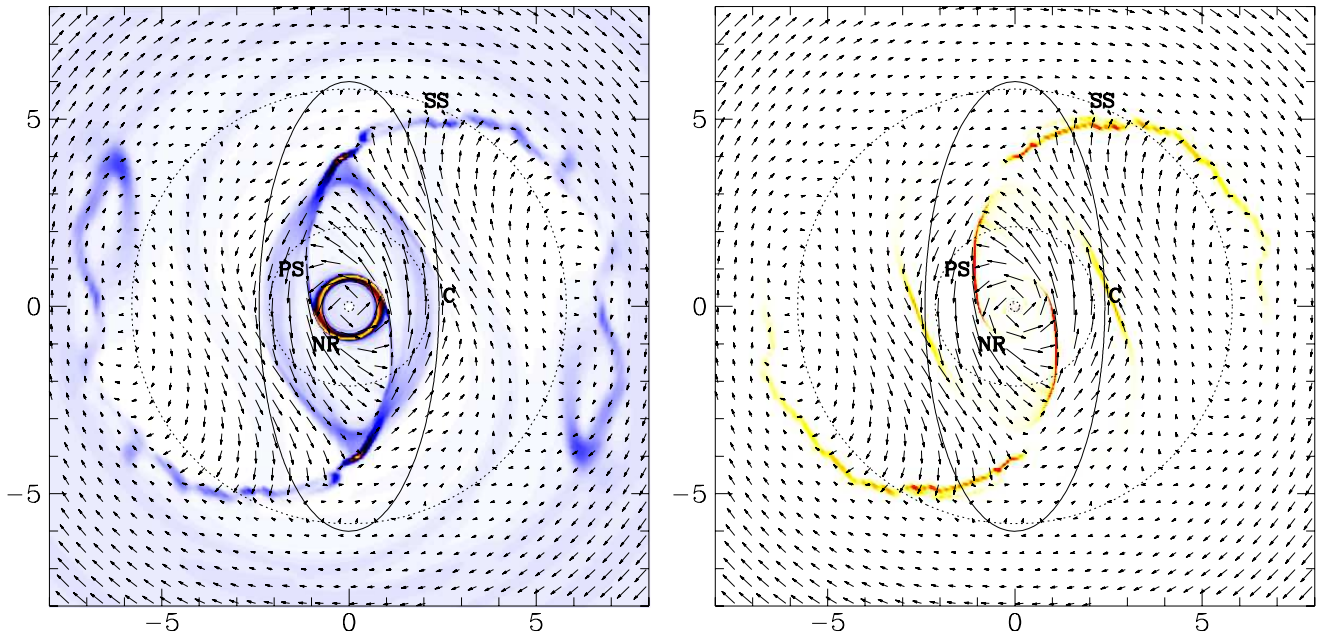

Figure 1. Density (*left*), and $div^2\mathbf{v}$ (*right*) snapshots for gas flow in a single bar (Model S05) on grid Hs made at time 1 Gyr. The bar, outlined by the solid line, is vertical. Dotted curves mark resonances in the azimuthally averaged potential. They are (innermost out): the inner ILR at 0.13 kpc, the outer ILR at 2.14 kpc, and the corotation at 7.78 kpc. Arrows mark velocity in the frame rotating with the bar, with length proportional to the speed. Bare arrowheads mark velocity direction only (in the case of small velocities near corotation). Positions of the principal shock (**PS**), nuclear ring (**NR**), spiral shock (**SS**), and the convergence region (**C**) are marked. In the density map, colours follow increasing densities from white through blue, black and red to yellow. The density saturates at 200 $M_\odot pc^{-2}$, and the **PS** is saturated in the divergence plot. Units on axes are in kpc.

Figure 2, we plot the gas density, and both components of velocity, for each zone at the radius 1.8 kpc at the same time as in Figure 1. The amplitude of the radial velocity is large: it varies between −140 and +140 km/s, more than half of the circular speed at that radius, and similar to earlier models. Nevertheless, the density peaks where the radial velocity is negative, and on average the inflow dominates.

The inflowing gas settles on near-circular orbits in the nuclear ring (**NR**), which in Fig.1 appears as a highly overdense region at radius about 0.9 kpc, with no evidence of strong shocks. Under a closer inspection, the nuclear ring has the appearance of a tightly wrapped spiral, as first noticed by Piner et al. (1995). In run S05 the ring extends between 0.8 and 1.3 kpc, and its position is independent of the resolution. Contrary to Piner's finding, the ring is not located at the maximum of the $\Omega - \kappa/2$ curve, which for Model 2 is at 0.55 kpc. The gas motion is mostly circular in the nuclear ring; there is no inflow beyond it, and gas accumulates there. Large densities and low shear in the nuclear ring make ideal conditions for star formation. If the gas density exceeds the critical value, self-gravity should become important, and star formation should occur.

No shocks cross the nuclear ring. There is only a very weak, tightly wound sound wave propagating inside the ring. Passing through the low-density gas there, it compresses it by a factor of 2, but does not appear to increase the inflow to the center: for the entire 2 Gyr of the run, the rate of inflow to the center is below $1 \times 10^{-4} M_\odot yr^{-1}$. Velocities inside the ring also remain mostly circular: close to the inner grid boundary at 0.1 kpc, the radial velocity is uniformly zero with largest deviations of 0.3 km/s, while the circular velocity is 80–100 km/s. In the next sections, we explore how to increase the inflow that is suspended by the nuclear ring.

In addition to the basic features above, Fig.1 indicates other generic characteristics of gas flow in a single bar. The principal shock is interrupted at about the position of the 4/1 resonance at radius between 3 and 4 kpc, where no large negative *div* **v** has been detected. At the same position, which is almost on the bar's major axis, the density plot shows high gas concentration, and the velocity vectors indicate no strong shear. Thus this is another region that may support star formation, as seen in NGC 1530 (Downes et al. 1996, Regan et al. 1996) and in M 94 (Waller et al. 2001). Englmaier & Gerhard (1997) explain the dynamics of this region by the interaction of gas moving on x_1 orbits with that on 4/1 orbits.

Outward of the 4/1 resonance, the principal shock continues as a weaker spiral shock (**SS**) that reaches the corotation radius, weakens there, and ends near the Lagrangian points L_4 and L_5. Gas entering the spiral shock mainly follows trajectories whose shapes indicate that they may be related to the banana orbits around these Lagrangian points (compare flow lines in *e.g.* Fig.3 and 13 of Athanassoula 1992). As first noted by Piner et al. (1995), here the lower-density pre-shock gas is deeper in the gravitational well than the dense gas past the shock, therefore Rayleigh-Taylor instabilities can develop and destroy the continuity of the shock.

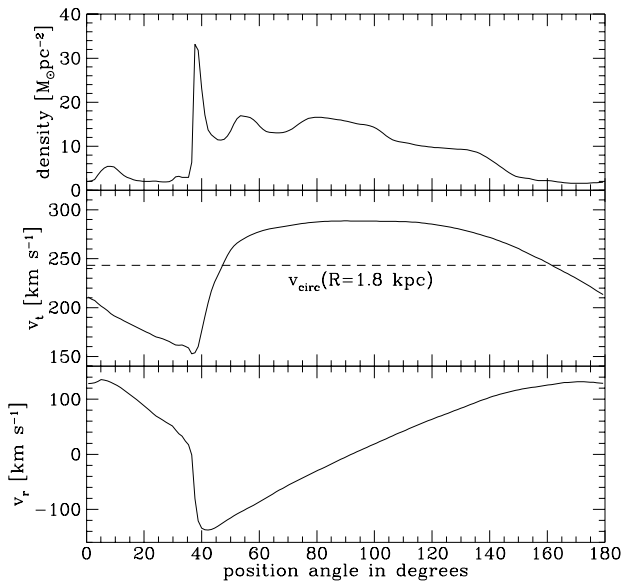

Figure 2. Gas density (upper panel) and both components of velocity (two lower panels) in gas flow in run S05 at the same time as in Figure 1 for each zone at the radius 1.8 kpc. The zones cover 180 degrees starting from the direction towards the bottom of the figure and going counterclockwise.

Gas on banana orbits runs against the shocked gas coming out from the principal shock, which creates convergence regions (**C**). This convergence funnels gas towards the 4/1 resonance at the end of the principal shock, which amplifies star formation there.

The existence of the principal and the spiral shocks, as well as of the convergence regions, is generic for various bar potentials, and independent of the sound speed in the ambient gas.

4 GAS FLOW INSIDE THE CENTRAL KPC

The exceptional resolution of a polar grid near its centre prompted us to investigate gas flows in the central kiloparsec of a barred galaxy. This resolution cannot be achieved on a fixed Cartesian grid. Also models using the SPH method experience a rapid drop of the particles onto the center, so any structure detected in the inner kiloparsec (Englmaier & Gerhard 1997, Patsis & Athanassoula 2000) cannot be followed for a long time. The CMHOG code allowed Piner et al (1995) to analyze and follow the nuclear ring in exceptional detail. Here, we use this code to investigate flows in the galaxy center that differ from Piner's model in properties of the gas and the underlying potential.

4.1 Dependence on gas sound speed

Englmaier & Gerhard (1997) have reported that when the gas in barred galaxies is modeled as an isothermal fluid, the flow morphology depends on the sound speed. They noticed that as the sound speed increases, the off-axis principal shocks seen in run S05 turn into shocks located almost on the bar's major axis, with no gas on the x_2 orbits. We performed a simulation in the same gravitational potential and initial conditions as in model S05, but with the gas sound speed increased to 20 km s^{-1}. A snapshot of gas flow in the run S20, which except for the higher sound speed does not differ from run S05, is presented in Fig.3. The principal shock persists, but moves closer to the bar's major axis, in agreement with models by Englmaier & Gerhard (1997). The outer spiral shock, and the convergent flow in the trailing side of the bar, retain their shape.

The change of sound speed has the most dramatic effect on the gas flow in the region of the nuclear ring. In the low-sound-speed run S05, the inflowing gas accumulates on the circular nuclear ring (Fig.1), and the principal shocks do not penetrate into the ring. Gas orbits in and inwards the ring are almost circular. At the high speed of sound (run S20), the nuclear ring turns into a nuclear spiral, with pitch angle higher than those of the nuclear ring and of the spiral inside it in run S05. The principal shock continues without substantial weakening along the nuclear spiral, which allows gas inflow all the way to the galaxy center. The inflow through the inner boundary rapidly increases from 1×10^{-4}M$_\odot$yr^{-1} at times before the spiral shock reaches the boundary, to 5×10^{-3}M$_\odot$yr^{-1} at time 0.14 Gyr, when the boundary is crossed. Results after the time when the shock crosses the inner boundary have to be interpreted with caution. Nevertheless, the inflow rate keeps increasing, reaching 0.15 M$_\odot$yr^{-1} at the end of the run S20 at 0.9 Gyr. We are currently working on following this mode of gas flow properly for longer times, but even this model, spuriously affected by inner boundary conditions, shows that the spiral preserves its shape throughout the run. It slightly tightens and becomes considerably denser: at 0.5 Gyr, the radial density distribution peaks at 330 M$_\odot$/pc^2, but by the end of the run, at 2 Gyr, it is 5 times larger.

At the end of the run, the densest parts of the spiral reside at radii around 0.3 kpc, i.e. well inside the peak of the $\Omega-\kappa/2$ curve, contrary to the findings of Piner et al. (1995) that the nuclear ring occurs roughly at the maximum of the $\Omega-\kappa/2$ curve. The arguments based on the orbital structure, outlined in the Introduction, indicate that the nuclear ring or spiral needs an ILR in the bar to form. Here we find that the ring forms between the inner and the outer ILR, but its position depends on gas sound speed, and differs from the maximum of the $\Omega-\kappa/2$ curve. Also, there are no grounds for the condition postulated by Piner et al. under which the nuclear ring can form. The absence of the nuclear ring in their model 8, on which this condition is based, results from the potential that does not allow x_2 orbits (model 86 in Athanassoula 1992), and not from the shift in the $\Omega-\kappa/2$ curve.

In the picture presented by Englmaier & Gerhard (1997), the transition from an off-axis principal shock with a nuclear ring to an on-axis one with a straight inflow to the center is more or less continuous. By contrast, in our runs we observe a nuclear spiral at high sound speeds. The study of on-axis shocks is particularly difficult on polar grids, where special inner boundary conditions have to be adopted. In general, we confirm the findings of Englmaier & Gerhard (1997) that not only the underlying potential, but also the gas characteristics influence the morphology of the flow. We extend their conclusion to the inner kiloparsec of galaxies,

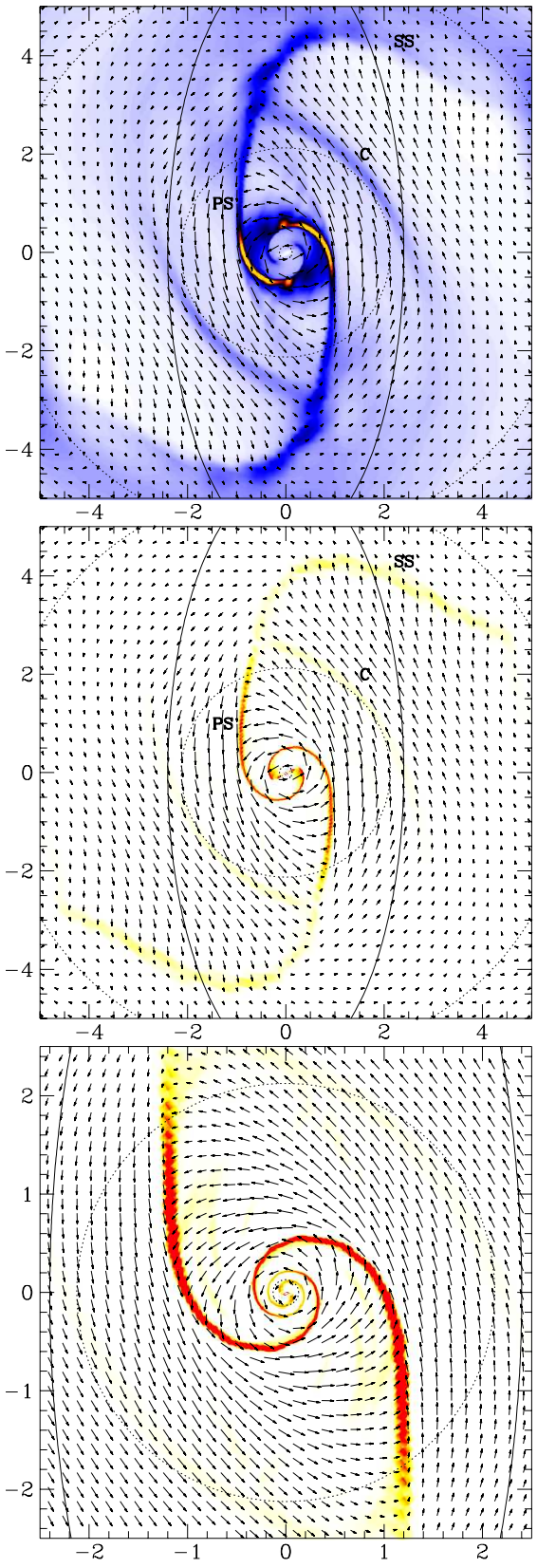

Figure 3. Gas flow in the inner regions of model S20 of a single bar on grid Me with density (the top panel), and $div^2\mathbf{v}$ (two lower panels), presented like in Fig.1. The two upper snapshots are taken at 0.195 Gyr, and the lower one at 0.135 Gyr, just before the spiraling shock crosses the inner grid boundary. Density saturates at 500 $M_\odot pc^{-2}$.

where the effect of the gas sound speed seems to be most dramatic. Inflow to the galaxy center, believed to be prohibited because of the orbital structure (gas accumulation on the nuclear ring) becomes possible when velocity dispersion of the clouds (equivalent to sound speed in the statistical interpretation) is large enough. Exploring variation of the gas flow with the sound speed shows that many qualitatively different morphologies of the flow can be produced in a given external gravitational potential. It is a promising way of looking for various modes of gas flow and morphology in central parts of galaxies. On the other hand, this shows that gas flows do not diagnose the potential uniquely.

4.2 A dynamically possible doubly-barred model

Finding particle orbits supporting doubly-barred systems proves difficult, since the potential is not steady in any reference frame, and therefore the Jacobi integral is no longer conserved. This might in principle mean that orbits are mostly chaotic, but in Paper I we showed that bars within bars have families of regular particle orbits that can support them. Further, the orbital structure puts strong constraints on sizes and rotation rates of the bars. Below we briefly review these constraints and their origins in order to show their role in shaping gas flows in double bars.

In Paper I, we approached the self-consistency issue by searching for potentials that generate orbits, with shapes such that the proper distribution of particles on these orbits could create the density distribution that gives rise to the assumed potential. As a first approximation, we assumed a potential of two rigid bars, rotating at two constant incommensurable pattern speeds. This a priori excludes full self-consistency, because two bars must distort and accelerate as they rotate through each other, but proves to be a useful approach to this complicated dynamical system, which successfully finds orbits supporting double bars.

In a single bar, the family of the x_1 orbits, that are aligned with the bar, forms the backbone of a steady potential, and particles trapped around orbits in the x_1 family provide building blocks for the bar. There is no such simple correspondence in a system consisting of two independently rotating bars, because the relative period of the bars adds an extra frequency to the system, and this frequency is generally incommensurable with the orbital periods there. Thus closed periodic orbits are extremely rare in double bars, i.e. they form a set of measure zero compared to the case of a single bar. Nevertheless, it is not the periodic orbits as such, but a proper distribution of particles trapped around them, that makes the building blocks of the potential. We looked for particles that together remain on a closed curve, which returns to its original position, after the two bars have come back to the same relative orientation, although the particles individually follow various not-closed orbits. We call such a curve *the loop*: stable loops, with shapes that follow the two bars in their motion, form the backbone of the pulsating potential in a doubly barred system. Particles trapped around such loops provide building blocks for a doubly barred galaxy. Fig.4 shows two examples of loops in a doubly barred galaxy as the bars rotate through each other — the loops change their shape as they follow the bars. One loop is following the main bar, and the other the secondary bar. The position of a randomly chosen particle

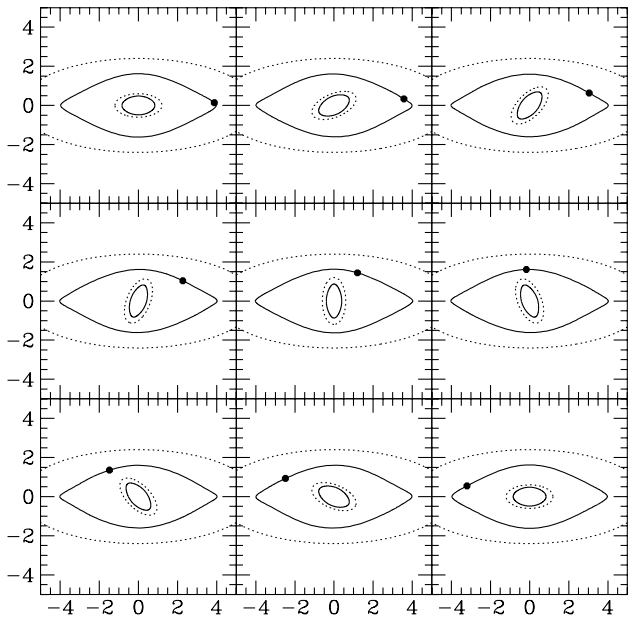

Figure 4. Time evolution of two loops (solid curves) in a doubly barred potential between two consecutive alignments of bars. Position of one arbitrary particle on the outer loop is followed and marked. Bars are outlined by dashed lines. Units on axes are in kpc.

from the outer loop is also marked. Note that although loops return to their original positions once the potential assumes its original shape, the particle ends up in a different place on the loop than it started from. Its orbit is not closed.

The concept of a loop proved to be essential to the realization that doubly barred galaxy potentials allow stable regular orbits that can support the shape of both inner and outer bars. In Paper I, we searched for models in which both bars have associated families of stable loops, that are elongated with the bar, and extend over the bar size. We found that this goal can be best achieved when the corotation of the inner bar overlaps with the ILR of the main one (which is the case of resonant coupling investigated by Tagger et al. 1987). In our nearly self-consistent model (Model 2 in Paper I) of a doubly barred galaxy, the most important loop families, which serve as the bars' backbones, correspond to the x_1 and x_2 orbits in the single bar. Loops supporting the main bar originate from its x_1 orbits, and loops supporting the secondary bar originate from main bar's x_2 orbits. Thus a secondary bar created in this way can exist only when there is an ILR in the main bar. Fig.9 of Paper I shows that only inner x_2 loops support the secondary bar in its motion. Thus the secondary bar ends well inside the ILR of the main bar, which also is the corotation of the secondary bar there. Therefore in the case of such resonant coupling, the secondary bar in Model 2 of Paper I is slow (it does not extend all the way to its corotation). This last finding may not be general though, since we assumed simple Ferrers' bars in Model 2. Considering bars with more realistic mass profiles could weaken the constraints found in Paper I. Nevertheless, the loop approach allows us to rule out, as being far from self-consistent, many hypothetical doubly-barred systems. The requirement of self-consistency puts strict limits on parameters of acceptable double bars. For this reason it is essential to examine gas flows in the dynamically possible Model 2.

4.3 Gas flows in a dynamically-possible double bar

We were exploring gas flows in a dynamically possible double bar by performing hydrodynamical runs in the potential of Model 2 constructed in Paper I. We present the gas flow in only one model of a double bar since it is the only near-self-consistent dynamical model yet constructed. The complicated dynamics of such systems makes generating such models a rather time consuming endeavour. Although we are not certain that our results are generic, we prefer to avoid investigating gas flows in arbitrary potentials of double bars, since the results may be misleading, as we do not know if such double bars can even exist.

Our main run D05 was performed for the gas sound speed 5 km s^{-1}. We also ran a model N05 in the potential of the secondary bar only, that is with the main bar density azimuthally averaged. We first focus on the results of the version of run D05, in which the secondary bar was introduced 0.5 Gyr after the primary. After that, we comment on the effects of simultaneous introduction of the bars. Run D05 has the same initial and boundary conditions as run S05, and the general features of the gas flow in this run remain unaffected by the presence of the secondary bar: the principal shock, the outer spiral shock, and the convergence region retain their shape and position. Also the appearance of the transient smudges is not affected by the modified potential, which implies that they are robust features, insensitive to model's details.

Fig.5 shows that, as expected, the secondary bar affects the central regions most strongly. The nuclear ring, clear and thin in the singly-barred run S05, is widened by the secondary bar (compare Fig.1 to Fig.5). After a 0.5 Gyr delay, which enables the nuclear ring in the primary bar to form, the secondary bar is introduced. Once the secondary bar reaches its full strength, at 0.56 Gyr, the inner part of the nuclear ring assumes an elliptical shape and begins to rotate with the secondary bar. Transitory elliptical rings (Fig.5 left) and shocks similar to the principal shocks in the primary bar (Fig.5 middle) form inside it at various times without a clear periodicity. Later during the run, the elliptical ring aligned with the secondary bar is established (Fig.5 right). The semi-minor axis of this ring is between 0.24 and 0.42 kpc — it does not extend all the way down the x_2 loop family, which ends at 0.17 kpc (Paper I). These late gas morphologies may be unrealistic, since they correspond to about 30 rotation periods of the secondary bar, while in the best N-body models so far the secondary bar survives only for several of its own rotation periods. On the other hand, our prescription for a nearly self-consistent double bar presented in Paper I should keep such a system indefinitely long.

If we introduce the secondary bar simultaneously with the primary at the beginning of the run, the ring associated with the secondary bar forms very early, already at 0.08 Gyr. It then follows the same evolution as the central regions in the version with the delayed introduction of the secondary bar. By the end of the run, the only difference in gas distribution is that the ring corotating with the inner bar is about

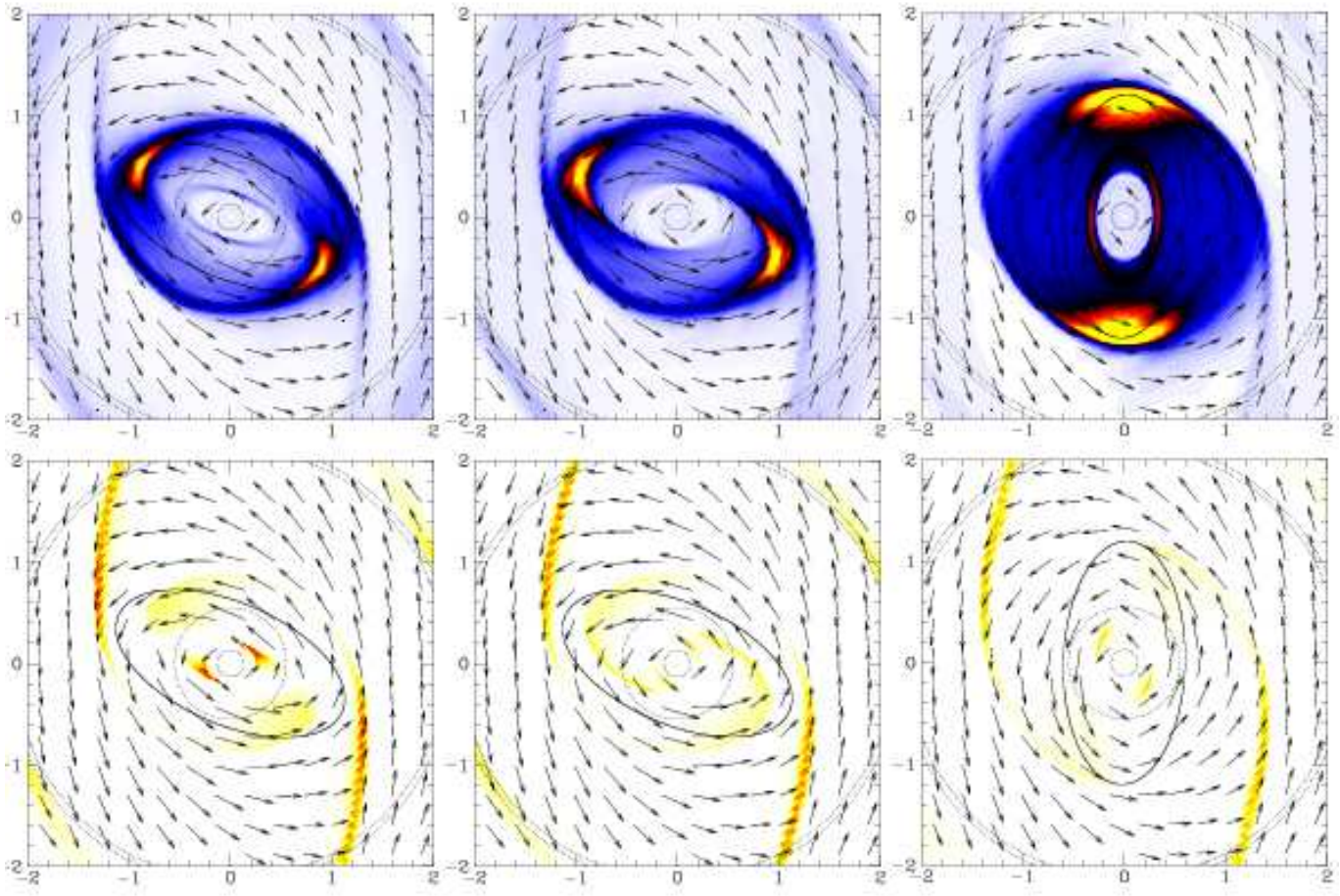

Figure 5. Like Fig.1, but for the model D05 of a doubly barred galaxy with the secondary bar being introduced at 0.5 Gyr. The three columns are close-ups of three different snapshots with density on the top and $div^2\mathbf{v}$ on the bottom. The snapshot on the left is taken at the time 0.695 Gyr, the one in the middle – at 0.780 Gyr, and the one on the right at 2 Gyr. The primary bar is always vertical, and the secondary bar is outlined by the solid line. Dotted lines indicate (innermost out) positions of the inner ILR of the main bar, the maximum of $\Omega - \kappa/2$ curve at 0.55 kpc, where the secondary bar is close to having an ILR, the outer ILR of the main bar, and the corotation of the secondary bar at 2.19 kpc. Density saturates at 400 $M_\odot pc^{-2}$.

50% denser in the version with the delayed secondary. All the morphology and kinematics is virtually identical, and the highest-density gas resides in 'twin peaks' on both ends of the secondary bar throughout both versions of the run.

Both versions of the run develop an elliptical ring or hole inside the secondary bar, which keeps gas away from the galaxy center. Once the secondary bar reaches full strength, gas inflow through the inner boundary is negligible, about 3×10^{-5} $M_\odot yr^{-1}$ in run D05, and gas cannot flow into the center. This contrasts with run S20 in a single bar, where some inflow was driven by a spiral shock. In the doubly barred potential, gas flow in the flattened nuclear ring is smooth, with only weak transient shocks being generated at a special relative position of the bars.

It is easy to understand this modeled flow in terms of the underlying orbital (loop) structure. In a singly-barred galaxy, gas follows stable closed periodic orbits, as long as they do not intersect or develop cusps. The principal shocks in a single bar develop because these orbits become cuspy or self-intersecting; they are offset because of the presence of the anti-aligned x_2 orbital family. Principal shocks are straight only in a bar that extends almost all the way to corotation. Similarly, in the potential of double bars, gas stays on or around the stable loops. In the dynamically possible Model 2 from Paper I, loops supporting the secondary bar extend only about half-way to its corotation radius, therefore we would not expect straight shocks, like the principal shocks in the main bar. Athanassoula (1992) found that even when the ratio of the bar size to its Lagrangian radius was lower than 0.71, the principal dust lanes curl around the bar, and start forming a ring. We do not expect off-centered shocks within the secondary bar, because no loops corresponding to the x_2 orbits in the secondary bar were found. An even stronger statement can be made: in the model we considered, the loops supporting the secondary bar originate from the x_2 orbits in the main bar – they are rather round, with no cusps, so there is no reason for shocks in the gas flow to develop. Thus we conclude that the gas flow in some self-consistent doubly barred galaxies may lack principal shocks or dust lanes. Nevertheless, this conclusion is based on one model only, and a better exploration of dynamically possible potentials is needed in order to reach firmer conclusions.

We performed an additional run to check to what extent the gas flows in the inner part of a doubly barred potential are due to combined action of both bars. In particular, we wanted to know, whether there can exist principal dust lanes in the small bar when the primary bar is absent. Run N05 has the same initial and boundary conditions as run D05, but here the primary bar is not included; we introduce the secondary bar alone. We found the gas flows in the inner part of the galaxy to be very similar to those in run D05 throughout the evolutionary time. Except for the absence of the nuclear ring, and lower peak densities in the gas (both evidently caused by the action of the primary bar, which is not present here), the gas flow in the secondary bar retains all the features of run D05.

5 DISCUSSION

5.1 General Remarks

Our high-resolution simulations of gas flow in barred galaxies allowed us to resolve and to follow features of the flow with exceptional detail. In Section 2.4 we noticed that the flow in a single bar never becomes fully stationary, and gas condensations propagate with unattenuated amplitude. If the bar is introduced more slowly, these features are weaker. We may speculate that irregular gas morphologies are more likely to appear in bars that formed fast, for instance as a result of interaction of two galaxies passing close to each other. We may see evidence of this effect in the interaction between NGC 1410 and NGC 1409, which perturbed the first galaxy, and probably led to star formation in its centre and at the 4/1 resonance along the bar. Blobs and smudges appear to connect the 4/1 resonances on the two opposite sides of the bar (Keel 2000).

5.2 Density-wave theory for non-self-gravitating gas in an imposed potential

Both runs in a single bar presented here display a spiral feature extending almost to the galaxy centre, but its appearance varies strongly with the gas sound speed. In the linear approximation, this spiral can be interpreted in terms of the gas density waves adopted by Englmaier & Shlosman (2000). In a standard density-wave theory for gaseous disks, the dispersion relation between the radial wavenumber k and the frequency ω is derived from the linearized continuity and Euler's equations (see *e.g.* Binney & Tremaine 1987, pp.355-359, hereafter BT). If these equations describe self-gravitating gaseous disks, then potential is coupled to density, and the linearized equations are homogeneous, with wave solution governed by the dispersion relation given by eq.(6-40) in BT for the limit of a tightly wound spiral.

Englmaier & Shlosman note that, unlike the standard density-wave theory, our case is the case of non-self-gravitating gas in an imposed potential. In this case, the potential term makes the linearized Euler's equations (BT eq.6-26) inhomogeneous, with non-wave solutions. A homogeneous counterpart of these equations, with no gravity term Φ_a, can be solved for a tightly wound spiral yielding the same dispersion relation as eq.(6-40) in BT, but with the gravitational constant $G = 0$. Since the wave frequency of an m-fold spiral is related to its pattern speed Ω_p by $\Omega_p = \omega/m$, the dispersion relation can be rewritten as

$$(\Omega + \kappa/m - \Omega_p)(\Omega - \kappa/m - \Omega_p) = \frac{k^2 v_s^2}{m^2}, \qquad (4)$$

where Ω and κ are the angular and epicyclic frequencies respectively, and v_s is the gas sound speed. Thus, for a given m, kv_s is a function of the imposed potential. Since the pitch angle i of the spiral at a given radius R is defined by $\tan i = |m/kR|$, in the tightly wound limit this angle is proportional to the sound speed v_s. Differentiating the dispersion relation (4) with respect to k shows that the group velocity of the wave ($v_g = \partial\omega(k,R)/\partial k$) can be written as the sound speed times a function of the potential. Several other interesting conclusions for non-self-gravitating spirals in realistic galactic potentials can be drawn from the dispersion relation (4). This relation prohibits the single-arm spirals in the inner part of the potential, since they can propagate only for $\Omega_p > \Omega + \kappa$ or $\Omega_p < \Omega - \kappa$. The $m = 2$ spiral is confined to within its own ILR, or outside its own OLR (Outer Lindblad Resonance), as originally noticed by Englmaier & Shlosman (2000). Higher-m spirals are confined inside their $\Omega - \kappa/m$ resonance or outside their $\Omega + \kappa/m$ one.

The inhomogeneous term in the Euler's equations comes from the external potential of the bar, and in the linearized form can be written as

$$\Phi_1 = \Phi_a(R)\cos(2\phi - 2\Omega_b), \qquad (5)$$

where Ω_b is the bar pattern speed. Although this term still bears a wave-like form, it no longer describes a tightly wound spiral, and one cannot use the approximations that led to the dispersion relation above. Nevertheless, solution of the linearized continuity and Euler's equations will return the coefficients of wave harmonics as functions of the imposed potential Φ_a. Only the $m = 2$ and $\omega = 2\Omega_b$ modes are driven by this form of the potential. In principle, other modes can propagate in the gas as well, but they will be damped numerically in the models, or by viscosity in real galaxies, and only the bar-driven modes will survive.

Therefore, in non-self-gravitating gas various spiral modes can propagate inside their own ILRs, but they will fade away unless something drives them. The only driven modes are those of $m = 2$ and $\omega = 2\Omega_b$, that is of a 2-arm spiral whose pattern is locked with the bar. This double-arm spiral will not extend beyond the ILR of the bar.

These conclusions are supported by our recent simulations of gas flow in very weak bars (Maciejewski 2001). The spiral pattern in the gas does not extend beyond the outer ILR, or within the inner ILR of the potential. Nevertheless, if we add a central black hole that removes the inner ILR, the spiral extends all the way to the inner grid boundary.

In the low sound speed run S05, the spiral is weak and rather tightly wound. It creates at most a factor of two density enhancement over the interarm region, and $div^2\mathbf{v}$ in the spiral is ten times smaller than in the principal shock. This spiral can be well understood in terms of the gas density waves. The nuclear spiral in this run terminates around the radius of 0.19 kpc, just outside the azimuthally averaged inner ILR of Model 2, as postulated by the linear theory above.

On the other hand, in the high sound-speed run S20,

the strong, loosely-wound spiral is a direct continuation of the principal shock – there is no nuclear ring to interrupt it. This generally agrees with the density wave theory, which postulates a higher pitch angle for a higher sound speed. Nevertheless, at 0.13 Gyr, just before the spiral collapses onto the center, the shock strength at the radius of 0.08 kpc, as measured by $div^2\mathbf{v}$, is only twice smaller than the average in the principal shock. The arm/interarm density ratio is as high as 10. This nuclear spiral reaches 0.05 kpc, almost three times closer to the nucleus than the position of the inner ILR. This nuclear spiral is definitely beyond the linear regime explored in the density-wave theory: there, sound waves cannot penetrate inward past the inner ILR, while the main shock in our model extends very close to the centre, crossing the inner ILR.

5.3 Relating observed and modeled features

In-spiraling shocks may in fact operate in real galaxies. Both Regan & Mulchaey (1999) and Martini & Pogge (1999) report an unexpectedly high frequency of nuclear spiral patterns in their samples, of 12 and 24 Seyfert 2 galaxies respectively. The patterns were detected by comparing visual with infrared HST images in combined color maps, and they indicate strong dust extinction in the spiral arms. Estimates of gas density based on this extinction lead Martini & Pogge to the conclusion that these spirals are caused by shocks in nuclear disks. The linear theory of gas density waves assumes low arm-interarm density contrast, with extinction smaller than 0.1 mag (Englmaier & Shlosman 2000), and no extensive star formation. The observed dust features can have $A_V \sim 0.5-1.5$ mag higher than the interarm region (Quillen et al. 1999), and the nuclear spirals show star formation (see *e.g.* Phillips et al. 1996; Laine et al. 1999).

The abovementioned two surveys of Seyfert 2 galaxy centers aimed to resolve the issue of the AGN feeding mechanism. Regan & Mulchaey (1999) searched for evidence of secondary stellar bars by looking for dust extinction in a form of straight lanes, analogous to the principal shocks in large-scale bars, which should be clearly seen in the color maps. Half of their sample shows nuclear spirals, and they report only three galaxies that have morphology consistent with gas flows in the bars. Out of those three galaxies, dust lanes in one (NGC 5347) are just continuation of the principal dust lanes in the main bar, another one (NGC 7743) shows a single straight dust lane on one side and circular dust morphology on the other. The only galaxy in that sample that is known to be doubly barred (NGC 3081) differs from the rest of the sample by virtue of having a central ring flattened along the secondary bar, and no straight dust lanes. This is just what our model D05 for a dynamically possible doubly-barred potential predicts. The outer parts of the NGC 3081 ring are blue – our simulations show that there is no shocks or strong shear there, so this is a possible site for star formation. Similarly, out of four best candidates for nuclear bars in the sample of Martini & Pogge (1999), two (NGC 5929 and Mrk 270) have no large-scale bar, out of which one (Mrk 270) shows straight dust lanes in the centre. A set of straight dust lanes in Mrk 471 is probably continuation from the large-scale bar. The case of the fourth candidate (Mrk 573) is complicated because of interaction between the disk and the ionization cone (Quillen et al. 1999).

Regan & Mulchaey take the lack of straight nuclear dust lanes to be evidence against the presence of secondary bars, and so they conclude that secondary bars are not a viable mechanism for feeding the active center of a Seyfert galaxy. Although our models confirm that the secondary bars may be inefficient in amplifying gas inflow to the galaxy centers, we also find that secondary bars do not have to reveal themselves through straight dust lanes — gas flows induced by them can be different from those caused by single (main) bars.

Finally, it is worth re-examining how the modeled features of gas flow in barred galaxies correspond with the best quality observations. Two major discrepancies arise here. First, we expect that strong shear in the principal shocks should prevent star formation there, while observations of early-type galaxies sometimes show strong Hα emission along the dust lanes (NGC 986, NGC 7582; Hameed & Devereux 1999). Second, observations of radio polarization in barred galaxies (Beck et al. 1999) show the regular magnetic field well aligned with the numerically modeled gas streamlines, while the depolarization region, expected around the principal shock, is shifted from it in the upstream direction by up to 0.9 kpc. Together, these two observations indicate that we are still far from the proper description of the postshock region in barred galaxies. Beck's observations of the magnetic field may also provide us with insight to the central galactic kiloparsec, where the field seems not to be aligned with the expected gas flow.

6 CONCLUSIONS

Using a high-accuracy hydrodynamical code, we investigated various modes of gas flow in a barred galaxy in an imposed gravitational potential of a single or double bar. We find that both circular motion of gas in the nuclear ring, and spiral shocks extending almost all the way to the galaxy center, are possible in a singly barred galaxy with an Inner Lindblad Resonance. At high sound speed, gas inflow to the center can proceed through the nuclear in-spiraling shock. At low sound speed the inflow is prevented by the nuclear ring.

It has been commonly assumed that the secondary bar embedded within a large-scale bar will generate gas flows, that are simply a small-scale analogue of those in the main bar (Regan & Mulchaey 1999). Models of arbitrarily chosen double bars (Maciejewski & Sparke 1997, Athanassoula 2000) are in accordance with this assumption, and they even predict periodic feeding of the nucleus by the inflow in the secondary bar. On the other hand, the loop approach that we developed in Paper I made clear that the potential adopted by Maciejewski & Sparke (1997) is unrealistic (Model 1 in Paper I).

Although we have constructed only one dynamically possible double-bar model (Model 2 in Paper I), and we cannot claim generality of our results, we argued that in this class of simple potentials, the orbital structure confines the secondary bar well within its corotation. The gas flow in this bar follows orbits that do not intersect or develop cusps. We have shown here that such a bar can bring gas

closer to the galactic center, but it does not create stationary shocks in the gas flow similar to the principal shocks in the fast-rotating main bar, neither does it enhance the gas inflow to the center. This conclusion, supported by observations of Seyfert galaxy centers, goes against the common expectation that secondary bars should activate a stronger inflow in barred galaxies. We find that the secondary bar can prevent, rather than enhance, the inflow.

ACKNOWLEDGMENTS

We would like to thank the referee, Jerry Sellwood, for useful remarks that lead us to clarify and improve this paper. WM would like to thank Mordecai-Mark Mac Low for the idea of examining shocks in the $div^2\mathbf{v}$ diagrams, Panos Patsis and Peter Erwin for useful discussions, and James Binney for comments on this manuscript. This research was partially supported by NSF Extragalactic Program grant AST93-20403. WM acknowledges a postdoctoral fellowship from the Max-Planck-Institut für Astronomie, Heidelberg, where part of the numerical simulations were performed.

REFERENCES

Athanassoula E., 1984, Phys. Repts., 114, 319
Athanassoula E., 1992, MNRAS, 259, 345
Athanassoula E., 2000, in Alloin D. et al. , eds, ASP Conf. Ser. Vol. 221, Stars, Gas and Dust in Galaxies: Exploring the Links. Astron. Soc. Pac., San Francisco, p.??
Beck R., Ehle M., Shoutenkov V., Shukurov A., Sokoloff D., 1999, Nature, 397, 324
Binney J., Tremaine S., 1987, Galactic Dynamics, Princeton Univ. Press, Princeton
Buta R., 1986, ApJS, 61, 609
Buta R., 1995, in Buta R. et al. , eds, ASP Conf. Ser. Vol. 91, Proc. IAU Colloq. 157, Barred Galaxies. Astron. Soc. Pac., San Francisco, p.11
Buta R., Crocker D.A., 1993, AJ, 105, 1344
Downes D., Reynaud D., Solomon P.M., Radford S.J.E., 1996, ApJ, 461, 186
Elmegreen B., 1997, ApJ, 477, 196
Englmaier P., Gerhard O., 1997, MNRAS, 287, 57
Englmaier P., Shlosman I., 2000, ApJ, 528, 677
Erwin P., Sparke L.S., 1999, ApJ, 521, L37
Friedli D., 1996, in Buta R. et al. , eds, ASP Conf. Ser. Vol. 91, Proc. IAU Colloq. 157, Barred Galaxies. Astron. Soc. Pac., San Francisco, p.378
Friedli D., Martinet L., 1993, A&A, 277, 27
Hameed S., Devereux N., 1999, AJ, 118, 730
Keel W.C., 2000, BAAS, 197.3701
Laine S., Knapen J.H., Pérez-Ramírez D., Doyon R., Nadeau D., 1999, MNRAS, 302, L33
Maciejewski W., 2001, in Knapen J.H. et al. , eds, ASP Conf. Ser., The central kpc of starbursts and AGN: the La Palma connection. Astron. Soc. Pac., San Francisco
Maciejewski W., Sparke L.S., 1997, ApJ, 484, L117
Maciejewski W., Sparke L.S., 2000, MNRAS, 313, 745 (Paper I)
Martini P., Pogge R.W., 1999, AJ, 118, 2646
Padoan P., Jones B.J.T., Nordlund Å.P., 1997, ApJ, 474, 730
Patsis P.A., Athanassoula E., 2000, A&A, 358, 45
Phillips A.C., Illingworth G.D., MacKenty J.W., Franx M., 1996, AJ, 111, 1566
Piner B.G., Stone J.M., Teuben P.J., 1995, ApJ, 449, 508
Quillen A.C., Alonso-Herrero A., Rieke M.J., McDonald C., Falcke H., Rieke G.H., 1999, ApJ, 525, 685
Regan M.W., Teuben P.J., Vogel S.N., van der Hulst T., 1996, AJ, 112, 2549
Regan M.W., Mulchaey J.S., 1999, AJ, 117, 2676
Sellwood J.A., Wilkinson A., 1993, Rep. Prog. Phys., 56, 173
Shlosman I., Frank J., Begelman M., 1989, Nature, 338, 45
Tagger M., Sygnet J.F., Athanassoula E., Pellat R., 1987, ApJ, 318, L43
Teuben P., 1995, in Buta R. et al. , eds, ASP Conf. Ser. Vol. 91, Proc. IAU Colloq. 157, Barred Galaxies. Astron. Soc. Pac., San Francisco, p.299
Waller W.H., et al. , 2001, AJ, 121, 1395
Woodward P.R., Colella P., 1984, J. Comput. Phys., 54, 115